

Nanostructured TiO₂ cavitation agents for dual-modal sonophotocatalysis with pulsed ultrasound

U.S. Jonnalagadda^a, X Su^a, J.J. Kwan^{b,*}

^a School of Chemical and Biomedical Engineering, Nanyang Technological University, 62 Nanyang Drive, 637459, Singapore

^b Department of Engineering Science, University of Oxford, Oxford OX1 3PJ, United Kingdom

ARTICLE INFO

Keywords:

Cavitation nuclei
Sonophotocatalysis
Pulsed ultrasound
Titanium dioxide nanoparticles

ABSTRACT

Current sonochemical methods rely on spatially uncontrolled cavitation for radical species generation to promote chemical reactions. To improve radical generation, sonosensitizers have been demonstrated to be activated by cavitation-based light emission (sonoluminescence). Unfortunately, this process remains relatively inefficient compared to direct photocatalysis, due to the physical separation between cavitation event and sonosensitizing agent. In this study, we have synthesized nanostructured titanium dioxide particles to couple the source for cavitation within a photocatalytic site to create a sonophotocatalyst. In doing so, we demonstrate that site-controlled cavitation from the nanoparticles using pulsed ultrasound at reduced acoustic powers resulted in the sonochemical degradation methylene blue at rates nearly three orders of magnitude faster than other titanium dioxide-based nanoparticles by conventional methods. Sonochemical degradation was directly proportional to the measured cavitation produced by these sonophotocatalysts. Our work suggests that simple nanostructuring of current sonosensitizers to enable on-site cavitation greatly enhances sonochemical reaction rates.

1. Introduction

Inertial cavitation is often attributed as the main driving force to facilitate sonochemical reactions [1,2]. For inertial cavitation to occur, ultrasonic waves in the fluid medium nucleate gas or vapor cavities to further undergo oscillations that can ultimately lead to bubble collapse at high acoustic intensities [1–3]. These collapse events create short-lived local regions of extreme temperatures and pressures [4], generating light—referred to as sonoluminescence—and reactive chemical species (e.g., free radicals, singlet oxygen, etc.) [3,5]. The use of ultrasound to generate these transient, high energy events is distinct from conventional synthetic chemistry methods and has allowed for the development of unique materials under ambient conditions [6,7]. Thus, sonochemistry has shown potential in a broad spectrum of applications including green polymer synthesis [8], waste water treatment [9], and biomedical therapies [10–12].

Considering that cavitation is a stochastic process and spatiotemporally random in homogenous fluids [3,13], conventional sonochemical methods rely on continuous wave ultrasound for prolonged periods of time (up to hours in some instances) to yield enough product.

Prolonging ultrasound exposure time, however, is energetically costly and may lead to secondary effects [2] and side reactions [8]. For instance, low frequency ultrasound (20–100 kHz) may promote polymer chain growth, but as reaction time increases it has also been shown to promote polymer degradation [8]. Higher frequency ultrasound (greater than 200 kHz) may circumvent polymer degradation. However, these acoustic waves are more readily absorbed by the fluid, leading to greater changes in fluid temperature that may influence the chemical reaction [14]. Extending ultrasound exposure times therefore may not lead to efficient product yield, and therefore alternative approaches to enhancing the sonochemical effect are under investigation.

To amplify the sonochemical effects of cavitation, photosensitizers such as photosensitive semiconductors [5,15–22], graphene [18,23,24], or polymers [25,26] have been used to promote radical species generation. Sonoluminescence from cavitation events in the fluid interacts with nearby photosensitizers to generate reactive oxygen species (ROS) [10,27,28]. Modifying the photosensitizers [23,28,29], adding hydrogen peroxide (H₂O₂), or including other stimuli (e.g., light) into the reaction solution have further enhanced ROS formation [30,31]. However, these methods lack spatiotemporal control of cavitation

Abbreviations: TFNs, TiO₂ fractured nanoshells; ROS, reactive oxygen species; MB, methylene blue; DPBF, 1,3-diphenylisobenzofuran; PSD, power spectral density; XRD, X-ray diffraction; HIFU, high intensity focused ultrasound; PCD, passive cavitation detector.

* Corresponding author.

E-mail address: james.kwan@eng.ox.ac.uk (J.J. Kwan).

<https://doi.org/10.1016/j.ultsonch.2021.105530>

Received 6 December 2020; Received in revised form 6 March 2021; Accepted 12 March 2021

Available online 17 March 2021

1350-4177/© 2021 The Authors.

Published by Elsevier B.V. This is an open access article under the CC BY-NC-ND license

(<http://creativecommons.org/licenses/by-nc-nd/4.0/>).

events; they rely on continuous wave ultrasound to nucleate and sustain cavitation. In order to control cavitation events at lower acoustic thresholds, exogenous gas bubbles have been demonstrated to function as cavitation nuclei (i.e., cavitation agents). These cavitation agents have been used in conjunction with photosensitizers recently to allow ROS generation with pulsed ultrasound [25]. Unfortunately, due to the limited fluence of sonoluminescence [32,33], this sonochemical method requires cavitation to occur nearby the photosensitizer to maximize light interaction. This spatial decoupling of inertial cavitation events from photocatalytic sites remains a key limitation for heterogenous sonochemistry. We hypothesize that synthesizing dual modality nanoparticles to control cavitation at photocatalytic sites will improve the rate kinetics of sonochemical reactions.

Recently, it has been reported that solid nano- and microparticles are also cavitation agents due to the gas trapped in pores and surface cavities [3,34,35]. In this report, we detail the synthesis of gas-trapping TiO_2 fractured nanoshells (TFNs) that function as a site for both the nucleation of cavitation and photocatalysis, thereby creating a sono-photocatalyst (Fig. 1a). TiO_2 is a well-documented material for photo- and sonocatalysis [5,15,16]. By inducing cavitation locally to the TFNs, sonoluminescence will more effectively activate the catalyst surface, thereby allowing *in situ* generation of radical species (Fig. 1b) [5]. These radicals may then react with other chemicals in the fluid media, such as methylene blue, to drive the reaction towards its products. Measurements of cavitation activity from the TFNs indicated that these particles nucleated cavitation at substantially lower acoustic intensities compared to pure water and gas-free TFNs (degassed TFNs). We then assessed sonochemical radical generation from TFNs exposed to pulsed ultrasound by measuring the decoloration of methylene blue (MB) and 1,3-diphenylisobenzofuran (DPBF). The subsequent cavitation energy suggested a correlation between cavitation from TFNs and the degradation of the molecular probes. Analysis of the sonochemical reaction kinetics revealed that the ultrasonic irradiation of the TFNs increased the degradation rate of MB by orders of magnitude compared to previously reported TiO_2 nanoparticles. Our results herein demonstrated that control of cavitation at photocatalytic sites by structuring the catalyst to

trap gas (e.g., TFNs) provided rapid radical formation at reduced power input. This approach may enable sustainable sonochemical methods for a broad range of unsustainable chemical reactions.

2. Materials and methods

2.1. TFNs hollow sphere synthesis

TFNs hollow spheres were formed by sol-gel template synthesis [36]. 10 wt% Polystyrene (PS) particles (300 nm, PL6003 Agilent, USA) were dispersed in absolute alcohol (107017 Millipore, 1:11 v/v) and sonicated for 10 min. The solution was then allowed to stir at 400 RPM while titanium butoxide (244112 Sigma, 0.2:2 in ethanol v/v) was added dropwise to the mixture. This solution was then sealed and allowed to stir for 2 h at room temperature, after which the particles were washed in ethanol by centrifugation at 4000 RCF for 10 min. After washing, the supernatant was removed and the particles were dried overnight at 60 °C to remove residual solvent, prior to calcination (5 °C/min temperature ramp) at 500 °C for 3 h, followed by air cooling to ambient temperature. The particles were then collected and stored in a dry cabinet at 30% humidity until ready for use.

2.2. TFNs characterization

The crystal structure of the TFNs particles was examined by X-ray diffraction (Bruker D2 Phaser) by $\text{Cu K}\alpha$ radiation with an accelerating voltage and current at 30 kV and 10 mA, respectively. The phase angle was adjusted between 5° and 40° at 0.05° increments ($2\theta = 10\text{--}80^\circ$) with a scan time of 0.5 s at each step.

The morphology of the particles was confirmed by field emission scanning electron microscopy (FE-SEM, JEOL JSM-6700, Japan) at an acceleration voltage of 5 kV and transmission electron microscopy (TEM, JEOL JEM-1400, Japan) was performed operating at 120 kV. The particle size was quantified by dynamic light scattering (DLS, Malvern Zetasizer) at 0.1 mg/mL concentration in aqueous media.

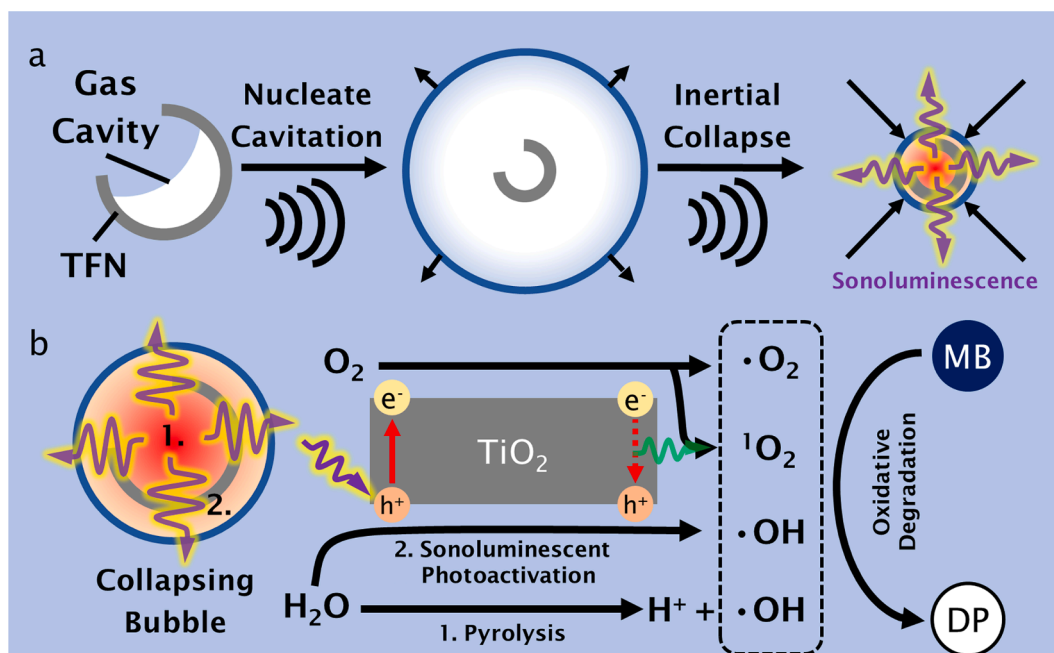


Fig. 1. Schematic diagram for TFNs mechanism of reaction. (a) Schematic illustration of gas entrapment by TFNs and generation of cavitation event by ultrasonic exposure. Upon bubble collapse, thermal effects, radical formation, and sonoluminescence are induced. (b) Pyrolysis of water caused by cavitation results in generation of H^+ and hydroxyl radicals. Sonoluminescence will result in photoactivation of the TiO_2 , further generating singlet oxygen and hydroxyl radicals. Chemicals in the fluid media, such as methylene blue, can interact with these newly generated radicals to accelerate chemical processing to degradation products (DP). (For interpretation of the references to color in this figure legend, the reader is referred to the web version of this article.)

2.3. TFNs solution preparation

TFNs particles were used at a 1 mg/mL working concentration in aqueous media. The particles were crushed with a microspatula into a fine powder within an Eppendorf tube prior to mixing with aqueous media placed in a sonicating water bath for 5 s further disperse the particles. To compare the sonochemical efficacy of the TFNs, commercially available TiO₂ powder (P25, Degussa) was similarly treated when preparing the working solutions. Solutions were then loaded into a continuous flow chamber for assessing the cavitation potential, or a static chamber for ROS identification by either light or ultrasonic irradiation (see relevant sections below).

2.4. Ultrasonic irradiation of TFNs solutions

A conventional HIFU setup was used in all HIFU experiments, and details of the setup are found in other reports [34,35,37]. In brief, a sine wave burst from a waveform generator was amplified by a 55 dB RF amplifier (Electronics and Innovation 1040L, Rochester NY) and passed through an electrical impedance matching network before reaching the HIFU transducer (1.1 MHz, Sonic Concepts, USA H-102 or 500 kHz, H-107). Any acoustic response from the sample during HIFU exposure was detected by the PCD (15 MHz, Olympus, Japan VU-V319). Irradiation parameters for both 1.1 MHz and 500 kHz were set to 45 msec pulse duration and a 33% duty cycle.

2.5. Cavitation detection and analysis

To identify the cavitation response from the TFNs system, the PCD data from each sine wave burst was processed by a power FFT to create a power spectral density (PSD) curve. For each burst, the integral of the PSD was computed and then summed across all the bursts to give the total received PCD signal energy proportional to the cavitation response for a given experimental run. To calculate the cavitation intensity for a given burst, the PSD integral was normalized to the PSD integral of degassed water irradiated with ultrasound under the same conditions [34,35,38].

2.6. Acoustic response

To assess the cavitation potential of the particles through a range of pressures, an acoustically transparent flow chamber was constructed, consisting of a 1 mm diameter channel in a 3 wt% agarose gel. 7 mL of the TFNs particle suspension was inserted into a 10 mL syringe and attached to a syringe driver to ensure continuous and constant flow through the channel at 500 μ L/min. The HIFU transducer focus was set to the centre of the chamber to irradiate the solution at 30 s intervals (20 cycles, 10 Hz PRF, 0.1–8 MPa Peak Negative Pressure for 1.1 MHz). The PCD signal was unfiltered, but all other experiments utilized an analogue 2.5 MHz high-pass filter (Allen Avionics F5286-2P50-B) before amplification through a broadband amplifier (5x, SRS SR445A). This processed signal was captured on the oscilloscope (National Instruments, USA PCI-5122) and saved for later processing as described previously [34,37]. The cavitation data was analyzed as described above using a threshold intensity of 6 dB and the probability of cavitation at each pressure level was quantified as the pulses greater than the cavitation threshold over the total number of pulses ($p(P) = \frac{P_{\text{pulses,cavitation}}}{P_{\text{pulses,total}}}$).

The cavitation threshold was calculated from the cavitation potential curve using a sigmoid fit ($p(P) = \frac{1}{1 + e^{-k(P - P_{50})}}$), where $p(P)$ is the cavitation probability for a given peak negative pressure, P , P_{50} is the pressure at which cavitation occurs 50% of the time and k is the intercept coefficient.

2.7. ROS identification

ROS identification was performed in acoustically transparent static chambers using a variety of model dyes. Methylene blue (MB) was used to demonstrate general oxidative degradation and 1,3-Diphenylisobenzofuran (DPBF) for singlet oxygen and superoxide anion detection in aqueous media. Where relevant, methanol was used as a hydroxyl radical scavenger by mixing into water at a 25 v%. Given that DPBF has limited water solution, a 1 mg/mL stock was prepared in DMSO, which was then diluted to 20 μ g/mL as the working concentration. MB working solutions were prepared at 5 μ g/mL, respectively. Working solutions of the dyes were then used to disperse TFNs particles at a 1 mg/mL concentration at 1 mL volumes in an Eppendorf tube. To enhance dispersity of the particles, samples were placed in a sonicating bath for 5 s before transferring the solution into the static chamber. The HIFU transducer focus was set to the centre of the chamber to irradiate the solution for 0, 0.5, 1.5, 3, 9, and 15 min in triplicate (50000 cycles, 33% duty cycle, 6 MPa). Control solutions were assessed without HIFU irradiation and particles. After irradiation, the solutions were collected from the reaction chamber and centrifuged to pellet the nanoparticles from the probe solution (see below).

To compare the effect of ultrasound to the more conventional photo-irradiation of the particles, 5 μ g/mL methylene blue solutions with 0–1 mg/mL TFNs were transferred into a 24 well plate and exposed to a 300 W xenon light source (~ 0.33 W/cm², $\lambda = 180$ –2000 nm). The wells were irradiated up to 30 min and 1 mL volumes were extracted for photo-degradation at 0.5, 1, 5, 10, 20, and 30 min.

Following photo-/sono-irradiation, all solutions were then centrifuged at 9000 RCF for 5 min to pellet the nanoparticles and the supernatant was collected for UV–vis spectroscopic analysis. DPBF and MB peak absorbances were detected at $\lambda = 420$ and 664 nm, respectively. The concentration versus time plots were curve fitted with an exponential decay to better visualize the reduction over time. The subsequent first order rate kinetics were calculated using an ordinary least squares linear regression according to the equation $-\ln\left(\frac{C_t}{C_0}\right) = kt$, where C_t is the concentration of dye at a given ultrasound exposure period, t is either the irradiation or exposure time, C_0 is the initial dye concentration at $t = 0$ min and k is the first order rate kinetics. To validate if a correlation was present with cavitation, the moles of dye degraded was calculated and plotted against cavitation response (see Section 2.5).

3. Results and discussion

3.1. Synthesis and characterization of TFNs

TiO₂ fractured nanoshells (TFNs) were synthesized by coating solid polystyrene particles with hydrolysed TiOH. These coated nanoparticles were subsequently calcinated at 500 °C to crystallize the titanium precursor and burn off the polystyrene core. Prior to calcination, the XRD spectra for titanium coated particles was assessed to be amorphous (Supplementary Fig. 1a), with the primary peak observed to come from the polystyrene core. Electron microscopy was performed to characterize the surface coating of the polystyrene particles; SEM images of the particles were observed to have a slightly rough surface (Supplementary Fig. 1b). TEM images suggested that the titanium precursor coated the polystyrene particles uniformly, evidenced by the darker rim contrast in Supplementary Fig. 1c–d. After calcination, the particle diameter reduced from 300 nm to approximately 260 nm. The crystal structure of the particles was confirmed to have formed a predominant anatase structure, reaffirming that the synthesis of TiO₂ occurred with minimal impurities (Fig. 2a) [39]. The hollow shell TiO₂ nanoparticles were then milled with a microspatula to fracture the shell and form the TFNs. The formation of TFNs was validated by SEM (Fig. 2b). Here, TFNs were observed to have a thin shell with some nanoparticles showing interstitial gaps in the shell. This was corroborated by TEM imaging, which

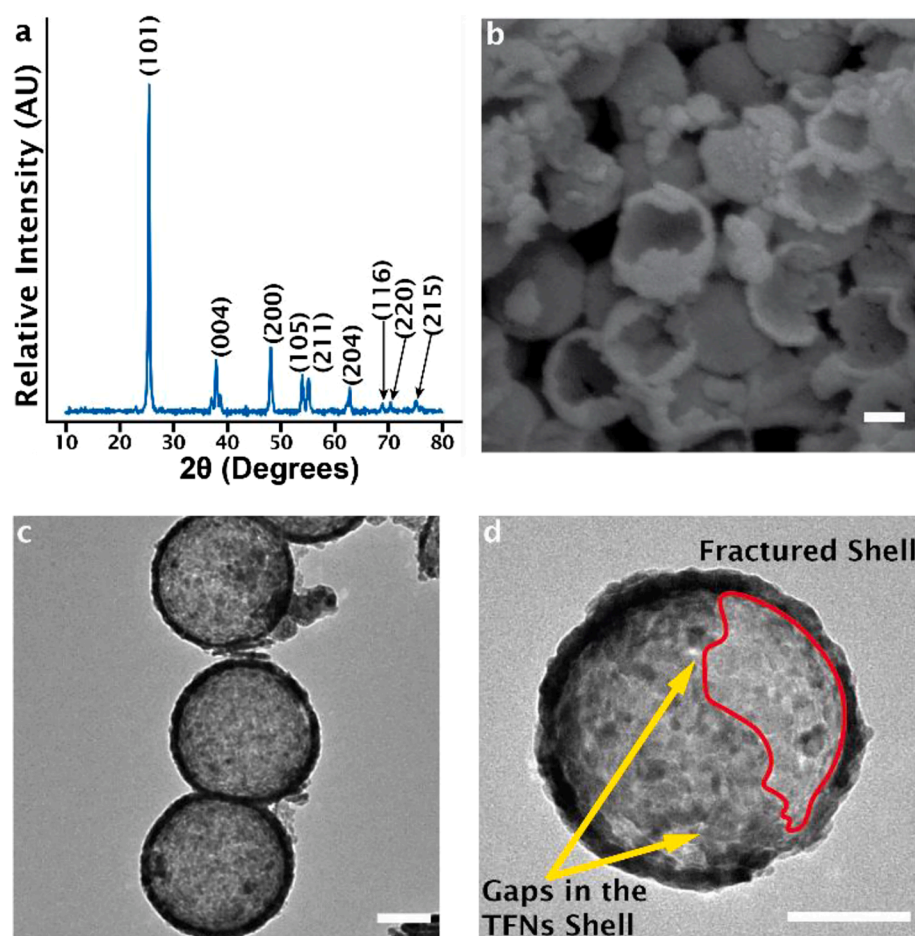


Fig. 2. Morphological and crystal characterization of TFNs particles. (a) Representative XRD spectra from TFNs. Peak locations matched well with anatase structure and planes are given for each peak. (b) SEM micrograph exhibiting TFNs surface structure to have a rough and “porous” morphology. Additionally, the particles assumed a mixture of fully formed, porous, and broken shell morphology. (c) By TEM imaging, the hollow TFNs structure is visualized by the contrast difference from the edge to particle centre. (d) Higher magnification TEM presented the fractured shell morphology of the TFNs (red outline) and gaps in the nanoshell can be further be observed as lighter pixel intensity spots (yellow arrows). Scale bars are 100 nm for all images. (For interpretation of the references to color in this figure legend, the reader is referred to the web version of this article.)

confirmed a hollow particle structure with a shell thickness of 15 nm, as evidenced by the pixel contrast difference between the particle edge to the centre (Fig. 2c). Higher magnification of TEM images of TFNs indicated the presence of large fractures and interstitial gaps in the shell (Fig. 2d), suggesting a quasi-porous structure of the TFNs. Some debris was observed in our micrographs, which might be attributed to fragments from the milling and solid TiO_2 particles that did not coat the polystyrene template.

3.2. Acoustic response of TFNs

Following synthesis and structural characterization, we next measured the acoustic cavitation response of TFNs to focused ultrasound in an agarose phantom at 1.1 MHz and 0.5 MHz through a range of voltages [35,37]. Given that the resultant pressure amplitude at the acoustic focus was frequency dependent, this voltage range corresponded to 0.5–8.0 MPa for the 1.1 MHz transducer and 0.1–3.9 MPa for the 0.5 MPa. The cavitation response was measured with a passive cavitation detector and normalized against a reference signal to obtain the power spectral density (PSD) curve. From these measurements, we calculated the probability for inertial cavitation at different acoustic pressure amplitudes for TFNs (1 mg/mL). A sigmoid function fit of the probability of cavitation indicated that the inertial cavitation threshold was approximately 4.8 ± 0.68 MPa peak negative pressure at 1.1 MHz (Fig. 3a). Deionized water and TFNs degassed by ethanol washes did not cavitate at any pressure amplitude tested at 1.1 MHz. At 0.5 MHz (Fig. 3b), the inertial cavitation threshold for TFNs was 3.5 ± 0.15 MPa peak negative pressure, which was substantially lower than at 1.1 MHz. The reduction in pressure amplitude for cavitation resulting from the decrease in ultrasound frequency was expected; lower frequencies have

a greater propensity to nucleate cavitation owing to the longer rarefactional period [14,40]. In our setup, water did not cavitate at either frequency for any pressure amplitude tested. Similarly, there was no detectable cavitation at any pressure amplitude tested for degassed TFNs exposed to 1.1 MHz ultrasound. In contrast, cavitation from degassed TFNs exposed to 0.5 MHz ultrasound was observed at higher pressure amplitudes, but the inertial cavitation threshold was never reached; the cavitation probability was less frequent and less intense than the TFNs under similar acoustic conditions. The reduced likelihood for cavitation from degassed TFNs suggested that cavitation from TFNs was due to gas entrapment on the surface of the nanoparticles. Therefore, all subsequent studies at 0.5 and 1.1 MHz were performed at 4.0 and 6.8 MPa respectively to maximize the presence of cavitation.

Compared to other solid cavitation agents of similar size, such as gold nanocones and polymeric nanocups, the cavitation threshold of TFNs was substantially larger [34,38,41]. This suggests that gas entrapment by the TFNs was not as efficient as other solid cavitation agents. This may be attributed to the varied morphology of the TFNs (Fig. 2b, c) [42]. Fractured nanoshells with cup shapes will behave similarly to polymeric cups when irradiated with ultrasound, which exhibit only inertial cavitation [38]. Other structures were observed to have gaps in the nanoshell, which will cause the TFNs to behave like mesoporous systems (e.g. mesoporous silica) [43]. For these TFNs structures, gas bubbles will be stabilized by the rigid and porous nanoshells, thereby substantially increasing the inertial cavitation threshold comparable to mesoporous silica [44].

In Fig. 3c, we visualized the PSD curves for each sample below, equal to, and above the cavitation threshold for TFNs. We observed that TFNs generated prominent harmonic noise when irradiated at 0.5 MHz, possibly due to the high intensity acoustic field being reflected by more

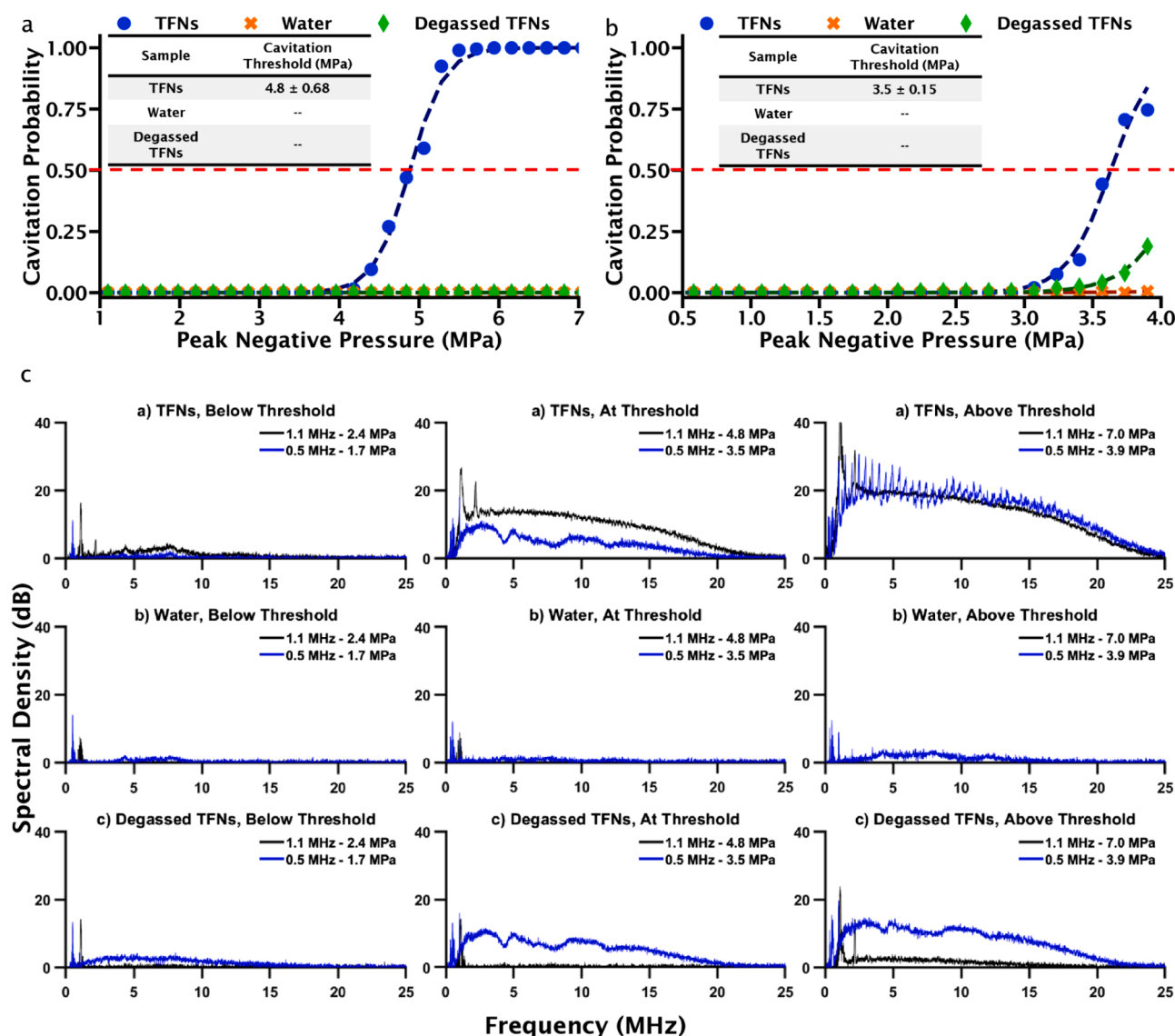


Fig. 3. Cavitation potential of TFNs at various acoustic pressures. Representative cavitation response for TFNs, water, and degassed TFNs is illustrated following irradiation (a) with a 1.1 MHz HIFU transducer and (b) a 0.5 MHz transducer for a range of pressures. The cavitation threshold was defined as the pressure at which the cavitation probability was 50%. The table inset in (a) and (b) describes the mean cavitation threshold and standard deviation from a triplicate for each sample. (c) The power spectral density was further analyzed to validate quality of noise (Below the cavitation threshold, all samples presented As the particles were excited above the cavitation threshold, the power spectral density curve expressed greater evidence of broadband cavitation at both frequencies. Comparatively, as cavitation was not as prominent for both the degassed TFNs and water only samples, the spectral curves did not present as strong broadband signals. (for a and b tables, $n = 3$, $\mu \pm \sigma$).

stable bubbles within the system [45]. The TFNs also generated significantly more broadband noise than either water or degassed TFNs at the same acoustic pressure amplitudes. This broadband noise, indicative of inertial cavitation, was in agreement with cavitation response of other solid cavitation agents comprising of cone and cup-shapes [34,38,41,45]. Here, inertial cavitation from our TFNs serves two purposes. First, bubble collapse nucleated from TFNs directly converts water into hydroxyl radicals [4,46], hydrogen peroxide [14,47] and other radicals [15] via pyrolysis. Second, sonoluminescence from a collapsing bubble is a source of light [48] for photocatalysis of water into the aforementioned chemical species and other free radicals. The proximity of cavitation events relative to the TFNs is important as it has been reported that sonoluminescent emissions follow isotropic radiation behaviour [32,33]. Therefore, cavitation away from the TFNs surface will limit light interaction with the particles and reduce the efficacy of ROS generation. By colocalizing bubble collapse at the TiO_2 surface, we

maximize the potential for sonochemistry from the collapsing bubble.

3.3. Catalytic function of TFNs

Once we confirmed that TFNs provided inertial cavitation in response to focused ultrasound, we next investigated the potential of the TFNs particles as sonophotocatalysts through degradation of MB and DPBF. Degradation of both MB and DPBF has already been investigated with photo- [24,25] and sonosensitizing agents [23,31,49]. MB was used as a model dye in our study as it belongs to a class of synthetic dyes that are non-biodegradable toxic runoff from the textile industry [24]. It is therefore highly desirable to develop sustainable techniques to degrade or remove this contaminant from water [23,24,30,49]. The chemical degradation of MB and similar organic pollutants occurs in the presence of various reactive oxygen species, such as hydroxyl radical and singlet oxygen. Thus, both photo- and sonocatalytic processes to break down

organic pollutants such as MB often seek to improve the ROS production rates.

3.4. Photocatalytic degradation of MB with TFNs

We next evaluated the photocatalytic activity of the TFNs by measuring the color degradation of MB using conventional light irradiation [50]. Solutions with or without TFNs underwent light irradiation with a xenon lamp ($\lambda = 180\text{--}2000\text{ nm}$) for up to 30 min (Supplementary Fig. 3a). From this, the first order rate kinetics for photodegradation of MB was assessed and tabulated (Fig. 4a). Adsorption of the dye by our particles was assessed in the dark over 30 min, where a minimal change in the MB concentration was found. In the absence of TFNs, there was gradual degradation of MB ($8 \times 10^{-3}\text{ min}^{-1}$) upon exposure to light. In stark contrast, the degradation of MB in solutions containing TFNs was more than two-fold faster ($18 \times 10^{-3}\text{ min}^{-1}$).

The photocatalytic degradation rate of MB from TFNs was orders of magnitude faster than other reported values for photocatalytic degradation of MB with TiO_2 (Supplementary Table 1). This enhanced rate may be attributed to the nanostructuring of the TiO_2 nanoparticles, allowing for greater surface area interaction with the reaction fluid. For example, Au decorated TiO_2 nanocups, which have a similar shape to our TFNs, degraded MB at a rate nearly 50% faster compared to Au decorated TiO_2 hollow spheres when exposed to light [17]. The reason for this enhanced photocatalytic capability was attributed to the unique shape of the nanocup, which allowed for more surface area for reactant/photon interactions in the concave portion of the cup and improved light scattering. The crystalline structure of TFNs may have also contributed to the enhanced generation of ROS. The anatase crystalline structure (Fig. 2a) within the TFNs has been shown to improve the oxidation of chemicals compared to other TiO_2 polymorphs, such as rutile [51]. Thus, the polymorph crystalline structure combined with the nanostructure of the TFNs synergistically promoted photocatalysis rates [17,52].

3.5. Sonophotocatalytic degradation of MB with TFNs

After confirming the photocatalytic capability of TFNs, the nanoparticles were assessed for their sonophotocatalytic performance by degrading MB within an acoustically transparent static reaction chamber (Supplementary Fig. 2). Different $5\text{ }\mu\text{g/mL}$ aqueous solutions of MB with TFNs, with degassed TFNs, or without TFNs were exposed to pulsed focused ultrasound for 0, 0.5, 1.5, 3, 9, and 15 min of ultrasound at a 33% duty cycle. The dynamics of these samples were compared to control samples, i.e., with or without TFNs in the absence of ultrasonic irradiation. We further evaluated the response of our system against commercially available P25 TiO_2 with ultrasonic irradiation at 1.1 MHz as a benchmark system [53–55]. The resulting color degradation at each total elapsed time point are shown in Supplementary Fig. 3b and Supplementary Fig. 3c for 1.1 MHz and 0.5 MHz irradiation, respectively. Because our approach utilized pulsed ultrasound, we evaluated the rate kinetics from both the total elapsed time (Supplementary Fig. 4) and ultrasound exposure time (33% of the elapsed time). For all tested conditions, negligible degradation of MB was observed except for TFNs solutions exposed to pulsed focused ultrasound. The degradation rate of MB with TFNs at 1.1 MHz (Fig. 4a) was calculated to be $475 \times 10^{-3}\text{ min}^{-1}$, a 59-fold increase compared to ultrasound only ($8.05 \times 10^{-3}\text{ min}^{-1}$) and a 5-fold increase compared to TFNs without ultrasound exposure ($82 \times 10^{-3}\text{ min}^{-1}$). Comparatively, reducing the frequency to 0.5 MHz (Fig. 4b) slightly increased the degradation rate with TFNs to $542 \times 10^{-3}\text{ min}^{-1}$. It is important to emphasize that the structure of the TFNs was unchanged following exposure to ultrasound and cavitation (Supplementary Fig. 5).

Degassed TFNs and P25 TiO_2 were also used to evaluate the importance of gas stabilization onto TiO_2 to facilitate the sonochemical degradation of MB. The degassed TFNs produced fewer cavitation events during irradiation, resulting in substantially slower degradation rates for both 1.1 MHz and 0.5 MHz frequencies ($139 \times 10^{-3}\text{ min}^{-1}$ and $60.5 \times 10^{-3}\text{ min}^{-1}$, respectively) compared to TFNs. Similarly, P25 TiO_2 displayed fewer cavitation events than TFNs and overall demonstrated similar behavior as the degassed TFNs and no TFNs control groups (Supplementary Fig. 6a).

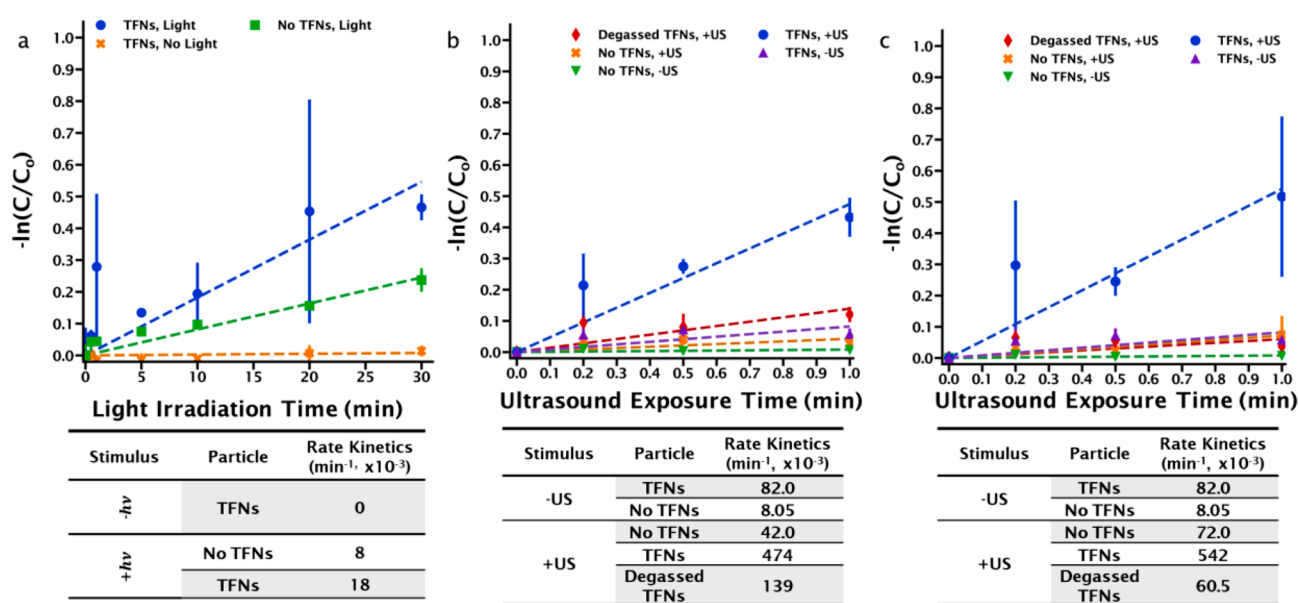


Fig. 4. Rate kinetics for MB photo/sonophotodegradation of TFNs particles. (a) Photocatalytic degradation of methylene blue probe was assessed over 30 min with or without TFNs in solution from which the first order rate kinetics were assessed for the total light irradiation time. Comparatively, the rate kinetics for sonocatalytic degradation of MB was assessed over the first 3 min of irradiation at (b) 1.1 MHz and (c) 0.5 MHz. Given the use of pulsed ultrasound, the first order rate kinetics was calculated as a function of ultrasound exposure time (33% total irradiation time). A tabulated summary of MB degradation rates at different stimuli and ultrasound frequencies is given in below the rate kinetics plots. ($n = 3$, $\mu \pm \sigma$). (For interpretation of the references to color in this figure legend, the reader is referred to the web version of this article.)

The intensity of inertial cavitation during sonochemistry is rarely quantified in current literature, though it is often accepted as the cause for sonochemistry. Here, we quantified the PCD signal energy from the reaction chamber, which was proportional to the cavitation response, for our sonodegradation experiments and correlate it to MB degradation for TFNs and controls (Fig. 5). These measurements indicated a direct positive correlation between cavitation energy and MB degradation for both 1.1 and 0.5 MHz (Fig. 5a and b, respectively). In Fig. 5a and b, we observed a linear correlation to the influence of cavitation on MB degradation with TFNs for both 1.1 and 0.5 MHz ($R^2 = 0.7$). Comparatively, degassed TFNs exhibited a weaker linear correlation for both frequencies ($R^2 = 0.5$ and 0.4 , respectively for 1.1 MHz and 0.5 MHz), while no TFNs and P25 displayed no correlation between cavitation and MB degradation (Supplementary Fig. 6b). The variation in the total PCD signal energy emitted by the samples are evident from the PSD heatmaps (Supplementary Fig. 7). This data was normalized against the free field reference to better visualize the acoustic intensity change over time during irradiation with either 1.1 and 0.5 MHz (Fig. 5c and d, respectively). For both frequencies, TFNs provided more intense and sustained cavitation signal compared to solutions without TFNs or with the degassed TFNs.

Interestingly, cavitation from ultrasound at 1.1 MHz provided more

degradation (Fig. 5a) compared to 0.5 MHz in the case of both fresh and degassed TFNs (Fig. 5b), despite the gradual decay in cavitation intensity at the higher frequency (Fig. 5c). At lower ultrasound frequencies, cavitation bubbles become larger [40], resulting in fewer, but more intense bubble collapses. Less frequent, more intense cavitation events may have therefore translated to less degradation of MB despite the high amount of measured cavitation response. Furthermore, bubbles may resist collapse all together or form cavitation clouds, which may reduce the intensity of sonoluminescence [40,46] at lower frequencies. At higher acoustic powers, cavitation will also occur more readily in the surrounding fluid, especially at lower frequencies (Fig. 5d), leading to multiple cavitation events away from TFNs.

Given that MB is commonly used as a model for assessing sono- and photocatalysis, we validated our approach against those used in literature as well as typical surface modifications that enhance the reactivity of TiO_2 (e.g., oxygen-deficient modification and hydrophilization). In order to more appropriately compare our approach against previous work, we quantified the rate kinetics proportional to the concentration of catalyst and reaction volume (Fig. 6, summary of data in Supplementary Table 2). We found that the rate kinetics from our approach was more than 1000-fold faster than other TiO_2 nanoparticles reported from existing literature at similar input power to the ultrasound transducer.

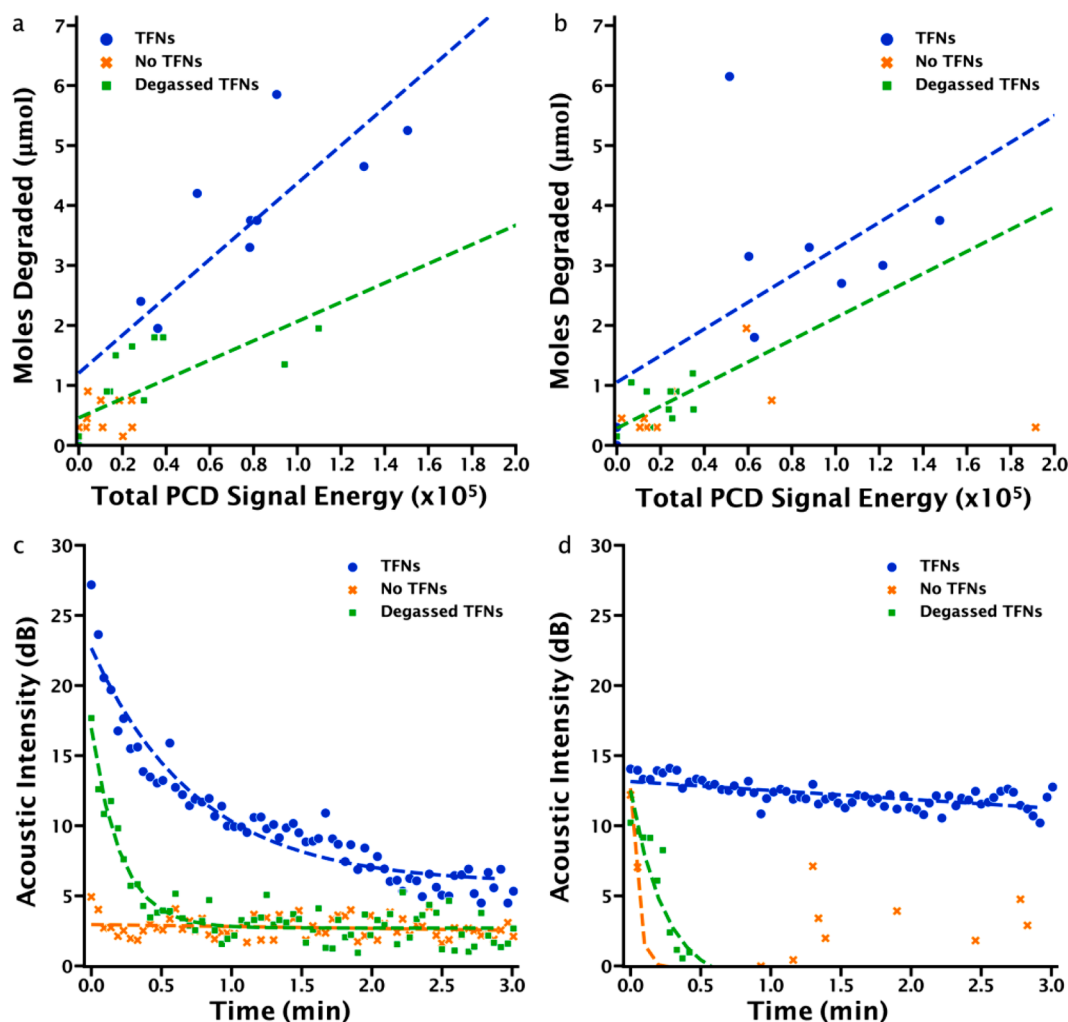


Fig. 5. TFNs cavitation dynamics and correlation to MB degradation. For the first 3 min of ultrasound irradiation, the PCD signal energy received (arbitrary units), which was proportional to the cavitation response, was quantified and correlated to the corresponding moles of MB remaining in solution. A linear regression was used to quantify the relationship between cavitation and probe degradation. (a) At irradiation with 1.1 MHz and (b) 0.5 MHz, it was observed that MB degraded proportionally to cavitation generated and this was accelerated by irradiation of the TFNs particles. The acoustic response of the particles was visualized by assessing the acoustic cavitation intensity vs time. When irradiated with either (c) 1.1 MHz or (d) 0.5 MHz, cavitation is more clearly sustained over longer exposure times with the TFNs compared to the degassed and no TFNs groups, leading to greater decolorization of the probe.

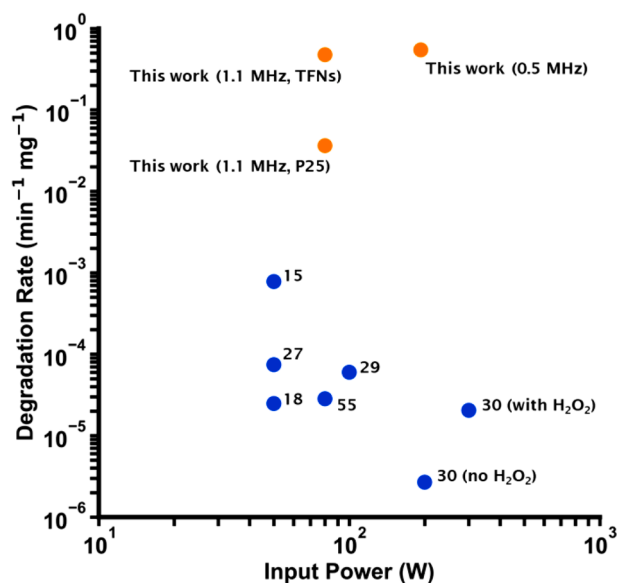


Fig. 6. Comparative overview TiO_2 nanoparticles for sonodegradation of MB. Rate kinetics comparing TiO_2 -based sonodegradation of MB between existing literature and the current work. Data is compiled from Supplementary Table 2, with each data point associated with its corresponding reference. Given variations in reaction volumes and particle/probe concentrations used, the rate kinetics was calculated proportionally to the particle mass used in the reaction container.

For degassed TFNs, cavitation was still observed, and subsequent analysis of the rate kinetics shown a reduction relative to fresh TFNs, but sonoreactivity was still at least 2 orders of magnitude greater than other reports (Supplementary Table 2). This difference in sonoreactivity with degassed TFNs was probably the result of residual surface nanobubbles on the nanoparticles, which may be present despite our attempts to degas and dewet the nanoparticles [56]. Interestingly, we observed that high frequency pulsed ultrasound irradiation of P25 particles resulted in over 1000-fold increase in the rate kinetics for MB degradation compared to a similar approach with P25 particles by Song *et al.* [55]. While there are distinct differences in the sonochemical reactor setup, this finding combined with our findings in Figs. 4 and 5 suggests that the acoustic field properties can influence and potentially enhance radical generation [2]. Likewise, when changing the nanostructure from the solid sphere morphology presented by P25 to a fractured nanoshell, we found a further 14-fold increase in the rate kinetics for MB degradation using the same acoustic parameters. Thus, our approach demonstrates the synergistic role in the acoustic field and sonocatalytic cavitation agents.

3.6. Sonophotocatalytic ROS generation from TFNs

To provide further evidence that TFNs sonochemically produced ROS, we assessed MB degradation with 25% methanol (Supplementary Fig. 8). Here, while cavitation was still observed, MB degradation was found to have reduced. As the reduction was non-zero, we suspect that MB degradation occurred as a result of hydroxyl radicals and other species generated by ultrasonic irradiation of TFNs. To validate this, we next assessed degradation of DPBF, an established probe for singlet oxygen detection, superoxide anion, and other ROS [16,25,57,58]. In Supplementary Fig. 9a, we observed complete degradation of the probe within 30 s of ultrasound exposure (equivalent to 90 s of elapsed time). Although ultrasound alone degraded the dye, the degradation rate was significantly slower than TFNs and generally more similar to the adsorption of the dye by the particles, which is approximately a 10% change over the total irradiation period. The rate kinetics for all conditions are summarized in the Supplementary Fig. 9b and

Supplementary Fig. 9c insets. In brief, TFNs exposed to ultrasound degraded DPBF at a rate of $7904 \times 10^{-3} \text{ min}^{-1}$, which was nearly 16-fold faster compared to ultrasound alone ($498 \times 10^{-3} \text{ min}^{-1}$). Similar to MB degradation, the breakdown of DPBF was proportional to the cavitation response in the reaction volume (Supplementary Fig. 9d). Interestingly, less cavitation energy was required to fully degrade DPBF compared to MB, leading to a more exponential change in degradation with cavitation energy. Though MB and DPBF were primarily studied in this report as a proof-of-concept, it is important to emphasize that this method to produce radical species to sonochemically accelerate degradation of other organic contaminants, such as rhodamine B, and may be useful for other advanced oxidative processes [15].

4. Conclusion

In conclusion, our approach of gas-stabilized TiO_2 nanoparticles allows for more effective sonochemical processing by colocalizing cavitation events at photocatalytic sites. By altering the acoustic field, we observed over a 1000-fold increase in the rate of degradation of MB using commercially available P25 nanoparticles compared to previous literature. When further manipulating the nanoparticle structure to afford greater gas bubble stabilization on the material surface, demonstrated that our TFNs reduced the acoustic energy required for nucleating cavitation, while simultaneously improving the rate kinetics of TFNs over P25 by approximately 14-fold and over 1000-fold compared to other methods. There was a direct positive correlation between cavitation response and chemical degradation, validating the importance of inertial cavitation for this sonochemistry. The TFNs survived exposure to both ultrasound and cavitation, suggesting the potential for recycling of the TFNs between sonochemical reactions. Work is currently underway in our laboratories to utilize these nanoparticles for augmented sonochemical conversion of intermediate reactants and promoting sonopolymerization.

Funding sources

Funding was provided by NTU start-up grant (M4081814.120).

Declaration of Competing Interest

The authors declare that they have no known competing financial interests or personal relationships that could have appeared to influence the work reported in this paper.

Acknowledgements

The authors thank Asst. Prof Paul Liu and QianWenhao Fan for use of their calcination furnace to synthesize the particles. The authors thank Assoc. Prof Xu Rong and Shuyang Wu for usage of their xenon lamp for the photodegradation studies. The authors further thank Lakshmi Deepika Bharatula for her assistance in devising the protocol for particle synthesis and in editing the manuscript.

Appendix A. Supplementary data

Supplementary data to this article can be found online at <https://doi.org/10.1016/j.ultsonch.2021.105530>.

References

- [1] K.S. Suslick, G.J. Price, Applications of ultrasound to materials chemistry, *Annu. Rev. Mater. Sci.* 29 (1) (1999) 295–326.
- [2] T.G. McKenzie, F. Karimi, M. Ashokkumar, G.G. Qiao, Ultrasound and sonochemistry for radical polymerization: sound synthesis, *Chemistry* 25 (21) (2019) 5372–5388.
- [3] R.G. Thomas, U.S. Jonnalagadda, J.J. Kwan, Biomedical applications for gas-stabilizing solid cavitation agents, *Langmuir* 35 (31) (2019) 10106–10115.

- [4] R.J. Wood, J. Lee, M.J. Bussemaker, A parametric review of sonochemistry: control and augmentation of sonochemical activity in aqueous solutions, *Ultrason. Sonochem.* 38 (2017) 351–370.
- [5] J. Bogdan, J. Plawinska-Czarnak, J. Zarzynska, Nanoparticles of titanium and zinc oxides as novel agents in tumor treatment: a review, *Nanoscale Res. Lett.* 12 (1) (2017) 225.
- [6] K.S. Suslick, J.R. Blake-Perutz, Y. Didenko, M.M. Fang, T. Hyeon, K.J. Kolbeck, W. B. McNamara, M.M. Mdeleleni, M. Wong, Acoustic cavitation and its chemical consequences, *Philos. Trans. R. Soc. London Ser. A* 357 (1751) (1999) 335–353.
- [7] H. Xu, B.W. Zeiger, K.S. Suslick, Sonochemical synthesis of nanomaterials, *Chem. Soc. Rev.* 42 (7) (2013) 2555–2567.
- [8] J. Collins, T.G. McKenzie, M.D. Nothling, M. Ashokkumar, G.G. Qiao, High frequency sono-ATRP of 2-hydroxyethyl acrylate in an aqueous medium, *Polym. Chem.* 9 (19) (2018) 2562–2568.
- [9] L. Parizot, T. Chave, M.-E. Galvez, H. Dutilleul, P. Da Costa, S.I. Nikitenko, Sonocatalytic oxidation of EDTA in aqueous solutions over noble metal-free Co₃O₄/TiO₂ catalyst, *Appl. Catal. B: Environ.* 241 (2019) 570–577.
- [10] Y. He, J. Wan, Y. Yang, P. Yuan, C. Yang, Z. Wang, L. Zhang, Multifunctional polypyrrole-coated mesoporous TiO₂ nanocomposites for photothermal, sonodynamic, and chemotherapeutic treatments and dual-modal ultrasound/photoacoustic imaging of tumors, *Adv. Healthc. Mater.* 8 (9) (2019), e1801254.
- [11] X. Wang, X. Zhong, L. Bai, J. Xu, F. Gong, Z. Dong, Z. Yang, Z. Zeng, Z. Liu, L. Cheng, Ultrafine titanium monoxide (TiO_{1+x}) nanorods for enhanced sonodynamic therapy, *J. Am. Chem. Soc.* 142 (14) (2020) 6527–6537.
- [12] X. Zhong, M. Zhang, Z. Tian, Q. Wang, Z. Wang, The study of enhanced high-intensity focused ultrasound therapy by sonodynamic N₂O microbubbles, *Nanoscale Res. Lett.* 14 (1) (2019) 381.
- [13] D.L. Miller, O.D. Kripfgans, J.B. Fowlkes, P.L. Carson, Cavitation nucleation agents for nonthermal ultrasound therapy, *J. Acoust. Soc. Am.* 107 (6) (2000) 3480–3486.
- [14] M.A. Beckett, I. Hua, Impact of ultrasonic frequency on aqueous sonoluminescence and sonochemistry, *J. Phys. Chem. A* 105 (15) (2001) 3796–3802.
- [15] J. Wang, Y. Guo, B. Liu, X. Jin, L. Liu, R. Xu, Y. Kong, B. Wang, Detection and analysis of reactive oxygen species (ROS) generated by nano-sized TiO₂ powder under ultrasonic irradiation and application in sonocatalytic degradation of organic dyes, *Ultrason. Sonochem.* 18 (1) (2011) 177–183.
- [16] D.G. You, V.G. Deepagan, W. Um, S. Jeon, S. Son, H. Chang, H.I. Yoon, Y.W. Cho, M. Swierczewska, S. Lee, M.G. Pomper, I.C. Kwon, K. Kim, J.H. Park, ROS-generating TiO₂ nanoparticles for non-invasive sonodynamic therapy of cancer, *Sci. Rep.* 6 (1) (2016) 23200.
- [17] J. Lu, P. Zhang, A. Li, F. Su, T. Wang, Y. Liu, J. Gong, Mesoporous anatase TiO₂ nanocups with plasmonic metal decoration for highly active visible-light photocatalysis, *Chem. Commun. (Camb.)* 49 (52) (2013) 5817–5819.
- [18] K. Zhang, F.J. Zhang, M.L. Chen, W.C. Oh, Comparison of catalytic activities for photocatalytic and sonocatalytic degradation of methylene blue in presence of anatase TiO₂-CNT catalysts, *Ultrason. Sonochem.* 18 (3) (2011) 765–772.
- [19] J.-Y. Jung, D. Lee, Y.-S. Lee, CNT-embedded hollow TiO₂ nanofibers with high adsorption and photocatalytic activity under UV irradiation, *J. Alloys Compd.* 622 (2015) 651–656.
- [20] R.S. Dariani, A. Esmaeili, A. Mortezaali, S. Dehghanpour, Photocatalytic reaction and degradation of methylene blue on TiO₂ nano-sized particles, *Optik* 127 (18) (2016) 7143–7154.
- [21] B.K. Mutuma, G.N. Shao, W.D. Kim, H.T. Kim, Sol-gel synthesis of mesoporous anatase-brookite and anatase-brookite-rutile TiO₂ nanoparticles and their photocatalytic properties, *J. Colloid Interface Sci.* 442 (2015) 1–7.
- [22] E. Thasirisap, N. Vittayakorn, P. Seeharaj, Surface modification of TiO₂ particles with the sono-assisted exfoliation method, *Ultrason. Sonochem.* 39 (2017) 733–740.
- [23] S. Sajjadi, A. Khataee, M. Kamali, Sonocatalytic degradation of methylene blue by a novel graphene quantum dots anchored CdSe nanocatalyst, *Ultrason. Sonochem.* 39 (2017) 676–685.
- [24] C.H. Nguyen, R.-S. Juang, Efficient removal of methylene blue dye by a hybrid adsorption-photocatalysis process using reduced graphene oxide/titanate nanotube composites for water reuse, *J. Ind. Eng. Chem.* 76 (2019) 296–309.
- [25] E. Beguin, S. Shrivastava, N.V. Dezhkunov, A.P. McHale, J.F. Callan, E. Stride, Direct evidence of multibubble sonoluminescence using therapeutic ultrasound and microbubbles, *ACS Appl. Mater. Interfaces* 11 (22) (2019) 19913–19919.
- [26] M.A. Margulis, I.M. Margulis, Contemporary review on nature of sonoluminescence and sonochemical reactions, *Ultrason. Sonochem.* 9 (1) (2002) 1–10.
- [27] Y.L. Pang, S. Lim, R.K.L. Lee, Enhancement of sonocatalytic degradation of organic dye by using titanium dioxide (TiO₂)/activated carbon (AC) derived from oil palm empty fruit bunch, *Environ. Sci. Pollut. Res. Int.* 27 (28) (2020) 34638–34652.
- [28] S. Liang, X. Deng, G. Xu, X. Xiao, M. Wang, X. Guo, P.a. Ma, Z. Cheng, D. Zhang, J. Lin, A novel Pt-TiO₂ heterostructure with oxygen-deficient layer as bilaterally enhanced sensitizer for synergistic chemo-sonodynamic cancer therapy, *Adv. Funct. Mater.* 30 (13) (2020).
- [29] E. Alves Nunes Simonetti, L.D.S. Cividanes, T.M. Bastos Campos, F. Williams Fernandes, J.P.B. Machado, G.P. Thim, Sonocatalytic degradation of methylene blue in the presence of TiO₂ doped carbon nanostructures—catalytic and adsorption comparison by different carbon forms, *Fullerenes Nanotubes Carbon Nanostruct.* 23 (8) (2015) 725–733.
- [30] N. Shimizu, C. Ogino, M.F. Dadjour, T. Murata, Sonocatalytic degradation of methylene blue with TiO₂ pellets in water, *Ultrason. Sonochem.* 14 (2) (2007) 184–190.
- [31] R. Balakumara, K. Sathya, R. Saravanamamizhan, Decolorization of methylene blue dye using sonocatalytic followed by photocatalytic process, *Water Conserv. Sci. Eng.* 1 (3) (2016) 161–166.
- [32] B. Boyd, S.A. Suslov, S. Becker, A.D. Greentree, I.S. Maksymov, Beamed UV sonoluminescence by aspherical air bubble collapse near liquid-metal microparticles, *Sci. Rep.* 10 (1) (2020) 1501.
- [33] M.P. Brenner, S. Hilgenfeldt, D. Lohse, Single-bubble sonoluminescence, *Rev. Mod. Phys.* 74 (2) (2002) 425–484.
- [34] J.J. Kwan, R. Myers, C.M. Coviello, S.M. Graham, A.R. Shah, E. Stride, R. C. Carlisle, C.C. Coussios, Ultrasound-propelled nanocaps for drug delivery, *Small* 11 (39) (2015) 5305–5314.
- [35] X. Su, R.G. Thomas, L.D. Bharatula, J.J. Kwan, Remote targeted implantation of sound-sensitive biodegradable multi-cavity microparticles with focused ultrasound, *Sci. Rep.* 9 (1) (2019) 9612.
- [36] J. Wang, J. Yu, X. Zhu, X.Z. Kong, Preparation of hollow TiO₂ nanoparticles through TiO₂ deposition on polystyrene latex particles and characterizations of their structure and photocatalytic activity, *Nanoscale Res. Lett.* 7 (1) (2012) 646.
- [37] U.S. Jonnalagadda, T.M. Nguyen, F. Li, J.H.C. Lee, X. Liu, A. Goto, J.J. Kwan, Sol-gel transitions of comb-like polymethacrylate copolymers by mechano-thermal stimuli in water, *Macromol. Chem. Phys.* 221 (13) (2020).
- [38] J.J. Kwan, G. Lajoinie, N. de Jong, E. Stride, M. Versluis, C.C. Coussios, Ultrahigh-speed dynamics of micrometer-scale inertial cavitation from nanoparticles, *Phys. Rev. Appl.* 6 (4) (2016).
- [39] C.J. Howard, T.M. Sabine, F. Dickson, Structural and thermal parameters for rutile and anatase, *Acta Crystallogr. Sect. B* 47 (4) (1991) 462–468.
- [40] A. Brothie, F. Grieser, M. Ashokkumar, Effect of power and frequency on bubble-size distributions in acoustic cavitation, *Phys. Rev. Lett.* 102 (8) (2009), 084302.
- [41] C. Mannaris, B.M. Teo, A. Seth, L. Bau, C. Coussios, E. Stride, Gas-stabilizing gold nanocaps for acoustically mediated drug delivery, *Adv. Healthc. Mater.* 7 (12) (2018), e1800184.
- [42] M.A. Chappell, S.J. Payne, The effect of cavity geometry on the nucleation of bubbles from cavities, *J. Acoust. Soc. Am.* 121 (2) (2007) 853–862.
- [43] J.L. Paris, C. Mannaris, M.V. Cabañas, R. Carlisle, M. Manzano, M. Vallet-Regí, C. C. Coussios, Ultrasound-mediated cavitation-enhanced extravasation of mesoporous silica nanoparticles for controlled-release drug delivery, *Chem. Eng. J.* 340 (2018) 2–8.
- [44] A. Yildirim, R. Chatteraj, N.T. Blum, A.P. Goodwin, Understanding acoustic cavitation initiation by porous nanoparticles: toward nanoscale agents for ultrasound imaging and therapy, *Chem. Mater.* 28 (16) (2016) 5962–5972.
- [45] C.D. Arvanitis, M. Bazan-Peregrino, B. Rifai, L.W. Seymour, C.C. Coussios, Cavitation-enhanced extravasation for drug delivery, *Ultrasound Med. Biol.* 37 (11) (2011) 1838–1852.
- [46] Y.T. Didenko, K.S. Suslick, The energy efficiency of formation of photons, radicals and ions during single-bubble cavitation, *Nature* 418 (6896) (2002) 394–397.
- [47] A. Weissler, Formation of hydrogen peroxide by ultrasonic waves: free radicals, *J. Am. Chem. Soc.* 81 (5) (1959) 1077–1081.
- [48] D.F. Gaitan, A.A. Atchley, S.D. Lewia, J.T. Carlson, X.K. Maruyama, M. Moran, D. Sweider, Spectra of single-bubble sonoluminescence in water and glycerol-water mixtures, *Phys. Rev. E* 54 (1) (1996) 525–528.
- [49] M. Fauzian, S. Jalaludin, A. Taufik, R. Saleh, Sonocatalytic methylene blue in the presence of Fe₃O₄-CuO-TiO₂ nanocomposites heterostructure, *J. Phys.: Conf. Ser.* 710 (2016).
- [50] H.N. Chang, S.X. Hou, Z.C. Hao, G.H. Cui, Ultrasonic green synthesis of an Ag/CP nanocomposite for enhanced photodegradation effectiveness, *Ultrason. Sonochem.* 40 (Pt A) (2018) 1039–1048.
- [51] T. Luttrell, S. Halpegamage, J. Tao, A. Kramer, E. Sutter, M. Batzill, Why is anatase a better photocatalyst than rutile?—Model studies on epitaxial TiO₂ films, *Sci. Rep.* 4 (1) (2014) 4043.
- [52] W.-T. Chen, A. Chan, V. Jovic, D. Sun-Waterhouse, K.-I. Murai, H. Idriss, G.I. N. Waterhouse, Effect of the TiO₂ crystallite size, TiO₂ polymorph and test conditions on the photo-oxidation rate of aqueous methylene blue, *Top. Catal.* 58 (2–3) (2014) 85–102.
- [53] C. O'Rourke, A. Mills, Probing P25 TiO₂ photocatalysis using photoinduced absorption spectroscopy (PIAS), *Chem. Commun.* 57 (10) (2021) 1242–1245.
- [54] T. Ohno, K. Sarukawa, K. Tokieda, M. Matsumura, Morphology of a TiO₂ photocatalyst (Degussa, P-25) consisting of anatase and rutile crystalline phases, *J. Catal.* 203 (1) (2001) 82–86.
- [55] L. Song, S. Zhang, X. Wu, Q. Wei, A metal-free and graphitic carbon nitride sonocatalyst with high sonocatalytic activity for degradation methylene blue, *Chem. Eng. J.* 184 (2012) 256–260.
- [56] B.M. Borkent, S.M. Dammer, H. Schonherr, G.J. Vancso, D. Lohse, Superstability of surface nanobubbles, *Phys. Rev. Lett.* 98 (20) (2007), 204502.
- [57] V.G. Deepagan, D.G. You, W. Um, H. Ko, S. Kwon, K.Y. Choi, G.R. Yi, J.Y. Lee, D. S. Lee, K. Kim, I.C. Kwon, J.H. Park, Long-circulating Au-TiO₂ nanocomposite as a sonosensitizer for ROS-mediated eradication of cancer, *Nano Lett.* 16 (10) (2016) 6257–6264.
- [58] T. Ohyashiki, M. Nunomura, T. Katoh, Detection of superoxide anion radical in phospholipid liposomal membrane by fluorescence quenching method using 1,3-diphenylisobenzofuran, *Biochim. Biophys. Acta* 1421 (1) (1999) 131–139.